HHS Public Access

Author manuscript

Biochim Biophys Acta. Author manuscript; available in PMC 2019 May 01.

Published in final edited form as:

Biochim Biophys Acta. 2018 May ; 1861(5): 481–496. doi:10.1016/j.bbagrm.2018.03.002.

Transcriptional regulation mediated by H2A.Z via ANP32e-dependent inhibition of protein phosphatase 2A

Hyewon Shin[1], **Minzhen He**[1], **Zhi Yang**[1], **Yong Heui Jeon**[1], **Jessica Pfleger**[1], **Danish Sayed**[1], and **Maha Abdellatif**[1,*]

[1]Department of Cellular Biology and Molecular Medicine, Rutgers University-New Jersey Medical School, Newark, NJ 07103

Abstract

The mechanisms that regulate H2A.Z and its requirement for transcription in differentiated mammalian cells remains ambiguous. In this study, we identified the interaction between the C-terminus of ANP32e and N-terminus of H2A.Z in a yeast two-hybrid screen. Knockdown of ANP32e resulted in proteasomal degradation and nuclear depletion of H2A.Z or of a chimeric green florescence protein fused to its N-terminus. This effect was reversed by inhibition of protein phosphatase 2A (PP2A) and, conversely, reproduced by overexpression of its catalytic subunit. Accordingly, knockdown of ANP32e inhibited phosphorylation of H2A.Z, whereas a mutation of serine-9 proved its requirement for both the protein's stability and nuclear localization, as did knockdown of the nuclear mitogen and stress-induced kinase 1. Moreover, ANP32e's knockdown also revealed its differential requirement for cell signaling and gene expression, whereas, genome-wide binding analysis confirmed its co-localization with H2A.Z at transcription start sites, as well as, gene bodies of inducible and tissue-specific genes. The data also suggest that H2A.Z restricts transcription, which is moderated by ANP32e at the promoter and gene bodies of expressed genes. Thus, ANP32e, through inhibition of PP2A, is required for nucleosomal inclusion of H2A.Z and the regulation of gene expression.

Keywords

yeast two-hybrid; MSK1; histone; chromatin immunoprecipitation

[*]To whom correspondence should be addressed: abdellma@njms.rutgers.edu. Tel: 9739721254.
Present address: Jessica Pfleger, Center for Translational Medicine, Temple University, Philadelphia, PA 19140

AVAILABILITY

Integrated genome browser [31] can be downloaded free at: http://bioviz.org/igb/Easeq [30] can be downloaded free at: http://easeq.net/

ACCESSION NUMBERS

The RNA polymerase II ChIP-Seq data (accession: GSE50637), and H2A.Z and Anp32e ChIP-Seq data (accession: GSE104702) are available in the GEO Datasets.

INTRODUCTION

The answer to the question of whether H2A.Z is involved in transcriptional activation or inhibition is not absolute, and depends on the species, cell type, gene, interacting proteins, and conditions. While in the protozoan *Tetrahymena thermophila*, Hv1 (the H2A.Z orthologue) is strictly localized to the transcriptionally active macronucleus [1], H2A.Z's relation with transcriptionally active genes in other eukaryotes is more complex. In yeast, Htz1 regulates the expression of active genes near the telomeres by suppressing Sir2- and Sir3-mediated spread of heterochromatin into those regions [2]. Conversely, Li et al show that Htz1 density is higher in intergenic compared to intragenic regions of genes, where it negatively correlates with transcriptional rates [3]. Furthermore, changes in growth conditions induces translocation of Htz1 from transcriptionally active to inactive genes [4]. More precisely, Htz1 is found at the TSS of nearly all genes in euchromatin, in the −1 and +1 nucleosomes flanking a nucleosome free region in the active genes, while present mainly in the −1 nucleosome in inactive genes [5]. The consensus from these studies is that Htz1 facilitates transcription via destabilizing the +1 nucleosome and/or preventing silencing factors such as Sirtuins from binding. The replacement of H2A for Htz1 is regulated by the SWR1 complex [6, 7], whereas, it removal requires INO80 [8]. On the other hand, in *Drosophila*, H2Av is present at thousands of both transcriptionally active and inactive genes in euchromatin, as well as, in heterochromatic chromocenter of polytene chromosomes [9]. Additionally, H2Av's density negatively correlates with that of pol II. Although this suggests transcriptional repression, more recently, it was shown that H2A.Z vs. H2A at the +1 nucleosome facilitates pol II progression [10].

In the mouse fibroblasts, chromobox 5 cooperates with H2A.Z to induce unique heterochromatin conformations, supporting a pro-inhibitory role of H2A.Z in gene transcription [11]. On the other hand, in murine embryonic stem cells, we see a dual functionality of H2A.Z, where in the undifferentiated state, H2A.Z, in conjunction with the polycomb subunit Suz12, is present at silenced homeodomain genes that are involved in cell differentiation. In contrast, in the committed neuronal progenitor cells, H2A.Z associates with highly expressed genes [12]. Similar to findings in yeast, it appears that the preferential loss of H2A.Z-containing nucleosomes is required for transcriptional activation during ES cell differentiation [13]. Also, H2A.Z requires SRCAP (SNF-2-related CREB-binding protein activator protein) and p400 [14], the human orthologues of Swr1, for its inclusion into nucleosomes [15]; and ANP32e [16, 17] or Ino80 for its exclusion [18]. In particular, it was previously shown that Anp32e directly interacts with the αC-helix of H2A.Z and induces its nucleosomal eviction, whereas, its knockdown promoted new H2A.Z binding sites at enhancers and insulators [16, 17].

The highly conserved, H2A.Z, has been also extensively studied in *Arabidopsis thaliana,* which provides further unique insight on its role in transcription. Interestingly, in this species, H2A.Z is present in the gene bodies of inducible genes, where it is responsible for their repression when unstimulated [19]. However, this pattern of distribution correlated with higher responsiveness of those genes to activating stimuli [20]. Additionally, this negatively correlated with gene body DNA methylation, suggesting that this modification plays a role

in excluding H2A.Z from gene bodies of constitutively expressed genes [20, 21]. However, this finding has yet to be verified in other species.

H2A.Z's stability is also subject to preferential regulation. In cardiac myocytes, we had previously shown that Sirt1 specifically induces proteasomal degradation of H2A.Z [22]. In this report, we show that ANP32e interacts with H2A.Z and is required for its stability through a PP2A and phosphorylation-dependent mechanism. Genome-wide distribution shows co-localization of the two molecules at the TSS of active genes, as well as, gene bodies of inducible and tissue-restricted genes, whereupon induction of growth results in differential changes in ANP32e levels and distribution, but minimal or no changes in H2A.Z, depending on the gene type.

MATERIAL AND METHODS

Animal care

All animal procedures used in this study are in accordance with US National Institute of Health *Guidelines for the Care and Use of Laboratory Animals (No. 85-23)*. All protocols were approved by the Institutional Animal Care and Use Committee at the Rutgers-New Jersey Medical School.

Culturing rat cardiac myocyte

Cardiac myocytes were cultured as described in our previous reports [23]. Briefly, hearts were isolated from 1 day old of Sprague-Dawley rats. After dissociation with collagenase, cells were subjected to Percoll gradient centrifugation followed by differential pre-plating for 30 min to enrich for cardiac myocytes and deplete non-myocyte cells. Myocytes were cultured in DMEM/F12 medium supplemented with 10% fetal bovine serum (FBS). All experiments were initiated after a 24 h culturing period.

Transverse aortic constriction (TAC) in mice

This was performed as described in our previous reports [24, 25]. Briefly, a 7-0 braided polyester suture was tied around the transverse thoracic aorta, against a 27-gauge needle, between the innominate artery and the left common carotid artery. Control mice were subjected to a sham operation involving the same procedure, minus the aortic constriction.

Echocardiography and Doppler

This was performed as described in our previous reports [24, 25]. Briefly, transthoracic echocardiography was performed using the Vevo 770 imaging system (Visual Sonics, Inc.) with a 707B-30MHz scanhead, encapsulated, transducer. Electrocardiographic electrodes were taped to the four paws, then one dimensional (1D) M-mode and 2D B-mode tracings were recorded from the parasternal short-axis view at the mid papillary muscle level. In addition, pulse-wave Doppler was used to measure blood flow velocity and peak gradient pressure in the aorta. For analysis, we used the Vevo 770 Software (Vevo 770, Version 23), which includes: analytic software package for B-Mode (2D) image capture and analysis; cine loop image capture, display, and review; software analytics for advanced measurements and annotations; and physiological data on-screen trace.

cDNA Library Construction and Screening Using the Yeast Two-hybrid System

The cDNA library was constructed and screened as described in our previous reports [26, 27]. Briefly, cDNA from 1–2-day-old neonatal rat hearts was subcloned into the pGAD10 vector upstream of the Gal4 activation domain, resulting in a library of ~2×10^6 independent clones with cDNA inserts that ranged in size from 0.5–4 kb. The bait consisted of the full-length H2A.Z downstream and in-frame with the GAL4 DNA binding domain in the pAS2.1 vector. Both the bait and the library were transfected into the yeast strain Y190 (*MATa, ura3-52, his3-200, lys2-801, ade2-101, trp1-901, leu2-3, 112, gal4*Δ, gal80Δ, cyh^r*2, LYS2::GAL1UAS-HISTATA-HIS3, URA3::GAL1UAS-GAL1TATA-LacZ*), using the BD Biosciences plasmid transfection kit. Positive interactions were selected for by tryptophan-, leucine-, and histidine-deficient plus 3-aminotriazol (-Trp, -Leu, -His+3AT) plating agar, and confirmed by *lacZ* expression. The library cDNA plasmid was isolated and then reintroduced into the yeast with the bait or control constructs to reconfirm the interaction before sequencing the insert.

Construction and delivery of recombinant adenovirus (Ad) vector

Recombinant adenoviral vectors were constructed, propagated, purified, and tittered as described in our previous reports [22, 26, 28]. Briefly, cDNA or shRNA were cloned into pDC315/316 or pDC311 shuttle (Microbix Biosystems Inc.), downstream of a CMV or a U6 promoter, respectively. These were transfected with the Ad5 virus backbone into 293HEK cells, in which the shuttle vector and the viral DNA recombined, introducing the DNA insert into the virus DNA. Single virus plaques were amplified in 293HEK cells, purified on a $CsCl_2$ gradient, dialyzed, and tittered on 293HEK cells with agarose overlay. Ad vectors were constructed with the following inserts, GFP, zGFP, GFPz, zGFPz, xGFPz, with the n-terminus, c-terminus, or both termini of H2A.Z, or the n-terminus of H2A.X and the c-terminus of H2A.Z, respectively, full-length H2A.Z, PP2Ac, ANP32e, ANP32e-GST, and short hairpin constructs targeting the Rattus norvegicus ANP32e (hairpin including a 6xT stop signal GACGGGGAGGAAGACGATGATTTCAAGAGAATCATCGTCTTCCTCCCCGTC and GATGAAGAAGACGATGATGATTTCAAGAGAATCATCATCGTCTTCTTCATC) and MSK1 (GAAGGGTTCTGCCTTCAGAATTTCAAGAGAATTCTGAAGGCAGAACCCTTC and ATCCTGTATACAATGCTGTCATTCAAGAGATGACAGCATTGTATACAGGAT), shaded area is the loop sequence. Cardiac myocytes were infected with 10–30 moi of the viruses for 24 h, as indicated in the figure legends.

Western blotting and antibodies

Proteins were extracted, 5–10 μg of the extract was analyzed on a 4 to 20% gradient SDS-PAGE (Criterion gels; Bio-Rad). The antibodies used for Western blot analysis included anti-H2A.Z (custom-made in-house, Rutgers University, see below), anti-ANP32e (Genway), anti-GFP (UC Davis, NIH neuroMab facility), anti-H2A.X (UpState Cell Signaling Solutions), anti-Cdk7, -MSK1, -ubiquitin, -H2A, -H2A.X, -pH2B, -Ac-H3, -pH3 (Santa Cruz Biotechnology), anti-phospho-p42/p44, -phospho-S6, -p42/p44, -S6, -pSer/pThr (Cell Signaling), and anti-Gapdh (Millipore).

Development of H2A.Z Monoclonal Antibody

The H2A.Z was developed in-house, as described in our previous report, using the H2A.Z C-terminal KLH-conjugated peptide (VIPHIHKSLIGKKGQQKTVC) as the immunogen [22]. After immunization of Balb/C mice, the mouse with highest antibody titer was used for fusion of the spleen cells with mouse myeloma cells Sp2/0 using standard hybridoma technique. The CELLine device CL-1000 (BD Biosciences) was used for producing high titer monoclonal antibody, which was purified using an Immunopure IgG purification kit (Pierce Biotechnology). The specificity of the antibody was verified using recombinant H2A (synthetic, ActiveMotif cat #31293) and H2A.Z proteins (expressed in E.Coli, ActiveMotif cat #31490), in addition, its reactivity was compared to ActiveMotif's anti-H2A.Z (anti C-terminus, cat #39943) (supplementary Fig. 1S).

Subcellular fractionation

Proteins were extracted and fractionated using the Subcellular ProteoExtract Kit (Calbiochem), per manufacturer's protocol. Ten μg of the extract was analyzed on a 4 to 20% gradient SDS-PAGE (Criterion gels; Bio-Rad).

ChIP-Seq and data analysis

Mice were subjected to TAC or a sham operation. After 7 days, cardiac function and structure were assessed by echocardiography, before isolation of the hearts. The hearts were then analyzed by anti-pol II (Abcam ab5095), anti-H2A.Z (ActiveMotif 39113), anti-Cdk9 (Santa Cruz sc-8338), and anti-ANP32e (Abcam ab5993) chromatin immunoprecipitation followed by next generation sequencing (ActiveMotif). Analysis of pol II ChIP-Seq is as described in our previous report [29]. The following applies to Cdk9, H2A.Z, and ANP32e ChIP-Seq (ActiveMotif). ChIP libraries were sequenced using NextSeq 500, generating 75-nt sequence reads that are mapped to the genome using BWA algorithms. The reads/tags were extended *in silico* by 150–250 bp at their 3′end (fragments), the density of which is determined along the genome, divided in 32 nt bins, and the results saved in bigWig and BAM (Binary Alignment/Map) files. Fragment peaks were identified using SICER, for which the term "interval" is used to define a genomic region with at least 3 consecutive peaks, while overlapping intervals are grouped into "active regions". The locations and proximities to gene annotations of intervals and active regions are defined and compiled in Excel spreadsheets, which include average and peak fragment densities. Regarding tag normalization and input control, the sample with the lowest number of tags is used for normalization of all samples, while the input is used to identify false positive peaks.

In addition, we separately analyzed the fragment densities by gene region, where the average value (Avg Val) of fragment densities at the TSS (−1000 to +1000) and in-gene/gene body (+1000 to 3′ end) regions for all genes were calculated separately. Subsequently, for sorting the genes by TAC/sham Avg Val of fragment densities for pol II, Cdk9, H2A.Z, and ANP32e at TSS and in-gene, the data from all samples were combined in a single excel file.

ChIP-Seq analysis software

The heatmaps, curves, and histograms shown in figure 8a–c, were generated using EaSeq [30]. Images of sequence alignments of fragments across chromosomal coordinates were generated using the Integrated Genome Browser (Fig. 8d–f, h–j) [31].

Statistical analysis

The significance of differences between 2 experimental groups was calculated using T-test (equal variance, 2-tailed), where $p < 0.05$ was considered significant.

RESULTS

ANP32e interacts with H2A.Z

We have previously shown that H2A.Z is involved in regulating cardiac myocyte growth [22]. To understand the mechanisms involved and the proteins that potentially interact with H2A.Z to mediate its function, we used it as a bait to screen a rat heart cDNA library using the yeast-two-hybrid system. This resulted in the identification of ANP32e as an interacting partner, through its C-terminal region (nt 680–1070 of NM_023210). This association has also been previously identified by Obri et al through a co-immunoprecipitation procedure [16]. To confirm the interaction, its specificity, and its site on H2A.Z, we generated Gal4-DB (DNA-binding domain) hybrid proteins with full-length H2A.Z, with it lacking the first 6 or 16 amino acids from its N-terminus domain (ΔN6 and ΔN16), with the first 16 N-terminus amino acids (NT) or the C-terminus of H2A.Z (CT), or full-length H2A.X. These constructs were transfected into yeast with the identified prey [Gal4-AD (activation domain)-ANP32e nt 680–1070]. Figure 1a shows that only yeast transfected with H2A.Z, delta N6, and NT grew on selective medium (-Leu-Trp-His) and expressed the Laz gene, both selection markers for detection of an interaction between bait and prey (Fig. 1a). This suggested that the interaction between H2A.Z and ANP32e occurs through the N-terminus of the former and the C-terminus of the latter, and is specific to H2A.Z.

To confirm the interaction in mammalian cells, we introduced ANP32e-GST (glutathione s-transferase) fusion protein or GST into cardiac myocytes. A pulldown with anti-H2A.Z co-immunoprecipitated ANP32e-GST, and conversely, a pulldown with anti-GST co-immunoprecipitation H2A.Z with the latter fusion protein (Fig. 1b). In addition, to confirm the interacting domain of H2A.Z, we generated green florescence protein (GFP) fusion proteins with either the N-terminus domain of H2A.Z (zGFP), its C-terminal domain (GFP-z), or both (zGFPz), or the N-terminal domain of H2A.X and the C-terminal of H2A.Z (xGFPz). Pulldown with anti-GFP shows that only the proteins with the N-terminal domain of H2A.Z co-immunoprecipitated ANP32e (Fig. 1c), confirming the N-terminal domain as the site of the interaction.

Knockdown of ANP32e induces nuclear exclusion and degradation of H2A.Z

To determine the effect of ANP32e on H2A.Z, we overexpressed or knocked down the protein in cardiac myocytes. Whereas the overexpression showed a dose-dependent increase in the protein in the cytosol, membrane, and nuclear fractions, it had no significant effect on the nuclear levels of H2A.Z (Fig. 2a). On the other hand, ~90% knockdown of ANP32e with

short hairpin RNA (shRNA, iANP32e) induced ~87% reduction in nuclear H2A.Z protein but not H2A.X (Fig. 2b–c), confirmed by a commercial anti-H2A.Z antibody (Fig. 2S) and a second independent shRNA (supplementary Fig. 3S). Also, see supplementary figure 7S, in which the H2A.Z protein signals on the Western blots, which are used for quantitation, have been demarcated. Knockdown of Anp32e did not reduce H2A.Z's mRNA levels (supplementary Fig. 4S), suggesting that it affects protein stability. In agreement, when epoxomicin was applied to inhibit proteasomal degradation of protein, we observed a full rescue of iANP32e-induced H2A.Z downregulation, however, it was not localized to the nucleus, but to the cytoskeletal fraction (Fig. 2b, 2d). Since ANP32e has been reported to inhibit protein phosphatase 2A [32], we used a general anti-pSerine/pThreonine (pSer/pThr) antibody to determine the effectiveness of its knockdown on phospho-protein modification. The figure shows a dramatic reduction in total cellular pSer/pThr content when ANP32e was reduced, and was not restored in the presence of epoxomicin. These results suggest that ANP32e is an inhibitor of pSer/pThr protein phosphatase, and is necessary for stability and nuclear localization of H2A.Z.

The N-terminus of H2A.Z confers ANP32e-dependent downregulation of proteins

To determine whether ANP32e knockdown-induced downregulation of H2A.Z was consistent with an interaction with its N-terminal domain, we tested the effect of ANP32e knockdown on the stability of the GFP fusion proteins described in figure 1c, including zGFP, GFPz, zGFPz, or GFP. In agreement, only constructs that harbor the N-terminus of H2A.Z (zGFP or zGFPz) were sensitive to ANP32e knockdown, exhibiting significant reduction of these proteins (Fig. 3a–b), but not mRNA levels (supplementary Fig. 4S). Particularly, the fusion H2A.Z-GFP proteins were found in all cell fractions including the nucleus, which exhibited the highest extent of reduction after ANP32e knockdown (Fig. 3b–c). Note that the GFPz and zGFPz fusion proteins were also detected by the anti-H2A.Z antibody specific for its C-terminus (Fig. 3b, third panel), which interestingly appears to have a higher affinity for the GFPz than anti-GFP. We also observed that the wild type GFP runs slower that the (z)GFP(z)-modified protein, which is plausibly due to an alternative upstream start site. These results confirm the role of N-terminal domain of H2A.Z in mediating ANP32e-induced stabilization of the protein.

Inhibition of PP2A by ANP32e prevents nuclear exclusion and degradation of H2A.Z

ANP32e belongs to a family of proteins that inhibit PP2A [33], and itself has been shown to inhibit PP2A during synaptogenesis [32]. Otherwise, we have little knowledge of the scope of its PP2A-dependent functions. To determine whether ANP32e knockdown-induced downregulation of H2A.Z is a PP2A-dependent activity, we delivered iANP32e to cardiac myocytes in the presence or absence of 10 nM of the protein phosphatase inhibitor, okadiac acid (OA, ID_{50} for PP2A is 1.6 nM and for PP1 is 315 nM [34]). Protein was extracted, fractionated, and analyzed by PAGE and Western blots. As seen in figures 4a and 4c, treatment with OA completely restored the iANP32e-induced reduction in the pSer/pThr content and nuclear H2A.Z. Conversely, overexpression of the catalytic subunit of PP2A (PP2Ac), reproduced the effects of ANP32e knockdown (Fig. 4b, 4c). In this experiment, we also added exogenous H2A.Z, as the excess protein is distributed to the cytosolic and cytoskeletal fraction, which allows us to correlate its stability with the presence of excess

PP2A in the different compartments. Similarly, the effects of PP2A on H2A.Z were reversed via inhibition of proteasomal degradation by epoxomicin, although, H2A.Z accumulated extra-nuclear. As with iAnp32e, PP2A did not have a significant effect on the mRNA levels of H2A.Z (supplementary Fig. 4S). These results suggest that ANP32e inhibits PP2A, protecting H2A.Z from direct or indirect dephosphorylation, nuclear exclusion, and proteasomal degradation.

ANP32e inhibits dephosphorylation of H2A.Z

H2A.Z is known to be modified via acetylation of lysine 4, 7, and 11 in the N-terminus tail. However, phosphorylation has not been identified as a modifier of H2A.Z. We detect posttranslational modification of the histone as an acidic shift on a 2-dimensional (2D) PAGE, which was eliminated by knockdown of ANP32e (Fig. 5a). To determine whether H2A.Z is a direct target of phosphorylation, we immunoprecipitated nuclear proteins from control- or iANP32e-treated cells with anti-pSer/pThr, followed by a 2D PAGE and anti-H2A.Z Western blot analysis. The results reveal that H2A.Z and H2A precipitated with anti-pSer/pThr, but only the former was abolished by iANP32e (Fig. 5a), suggesting that H2A.Z is phosphorylated and that ANP32e inhibits its dephosphorylation.

H2A.Z harbors a conserved serine-9 (Ser-9), positioned in the N-terminus tail between the acetylated lysine, and, thus, has the potential to modulate acetylation. To examine its role, we mutated the site into an alanine (A9) or aspartate (D9). Myocytes were treated with a control or adenoviral vectors harboring wild type, A9, or D9 H2A.Z for 24 h. Protein was extracted, fractionated, and analyzed by Western blots. The results revealed that the wild type H2A.Z construct increased nuclear and extra-nuclear protein levels, whereas, neither mutant increased nuclear H2A.Z levels, in spite of the fact that the mRNA levels were similar to wild type (supplementary Fig. 4S). When epoxomicin was added to the cells along with the viral constructs, we observed the accumulation of H2A.Z mutant proteins in the cytoskeletal fraction, but none in the nuclei. Although, we had anticipated that the D9 mutation may confer a phospho-mimic phenotype that would potentially have superior nuclear inclusion, however, this was not the case, instead the mutant functioned as a phospho-deficient protein. These data show that Ser-9 is required for the nuclear inclusion and stability of H2A.Z.

Knockdown of MSK1 induces nuclear exclusion of H2A.Z

Two known nuclear kinases include, the functionally redundant, mitogen and stress-induced kinases 1 and 2 (Msk1/2), which phosphorylate H3 [35]. Because of its known nuclear kinase function, we tested the idea that MSK1 regulates H2A.Z's nuclear inclusion and stability, via knockdown of the kinase. Short hairpin RNA targeting MSK1 (iMSK1) was delivered to the myocytes in a dose-dependent fashion for 24 h, in the presence or absence of epoxomicin. Protein was extracted, fractionated, and analyzed by PAGE and Western blots. MSK1 was found in the nuclear and the cytoskeletal fractions, with lower levels in the cytosol. Its knockdown significantly reduced nuclear H2A.Z, which was completely rescued by epoxomicin (Fig. 6a, red arrow pointing to second lane of the cytoskeletal fraction), but failed to localize to the nucleus, similar to what we see with the knockdown of ANP32e (Fig. 6). This effect was only seen with the lowest dose of iMSK1, whereas, the higher doses

appear to induce cell death, as evidenced by an increase in p-H2B. Thus, MSK1 plays a role in regulating H2A.Z's nuclear inclusion, however, we have no evidence that it directly phosphorylates H2A.Z.

ANP32e is required for the phosphorylation of signaling molecules and regulation of gene expression

ANP32e protein levels are highest in both the cytosol and nucleus, as seen in figures 2 and 4. Therefore, we anticipated that it would influence phosphorylation-dependent signaling through inhibition of PP2A, a function that has not been tested yet. Short hairpin RNA targeting ANP32e (iANP32e) was delivered to cardiac myocytes for 24 h, in serum starved conditions, after which they were stimulated with 10% fetal bovine serum (FBS) for 5 min. Protein was extracted, fractionated, and analyzed by PAGE and Western blots. ANP32e knockdown, near completely inhibited FBS-induced phosphorylation of erk1/2 and ribosomal S6 proteins in the cytosol and membrane fractions (Fig. 7a–b). Noteworthy, while total erk1/2 protein levels were unaffected, we observed >90% reduction in total S6 protein, specifically in the nucleus, following Anp32e knockdown. Also, note that several higher molecular weight bands were detected by the H2A.Z antibody that were eliminated by the shRNA. We speculate that these might be post-translationally modified variants of the histone. Thus, the data prove that ANP32e is required for FBS-induced phosphorylation of erk1/2 and S6. Furthermore, it suggests that ANP32e may play a role in selectively regulating gene expression/protein stability, including that of nuclear S6.

The presence of ANP32e in the nucleus, and its association with H2A.Z and promoting its phosphorylation and stability, would strongly suggest a role in regulating gene expression directly via regulating H2A.Z, or indirectly through regulating other nuclear factors' phosphorylation and stability. Cardiac myocytes respond to growth factor stimulation via an increase in mass and size, which is dependent on transcriptional remodeling. After delivery of iANP32e to the cells for 24 h, in serum free conditions, they were stimulated for an additional 24 h period with 10% FBS. In parallel, cells were treated with the PP2Ac overexpressing viral vector. Protein was extracted, fractionated, and analyzed by PAGE and Western blots. The results reveal selective ANP32e-induced modulation of gene expression (Fig. 7c–d). Specifically, neither iANP32e nor PP2Ac, affected the expression of endogenous H2A, Akt, nor acetylated-H3 content, but specifically reduced the basal and FBS-induced expression of Cdk7, a kinase required for transcription initiation, in addition to S6 observed in figure 7a. This suggests that ANP32e has selective direct or indirect effects of gene expression or protein stability.

ANP32e co-localizes with H2A.Z and is differentially regulated during growth

While we have established a physical and functional interaction between ANP32e and H2A.Z, we have yet to establish their relative spatial distribution across the genome, and how it may change during growth. To examine this, we performed chromatin immunoprecipitation (ChIP)-sequencing with anti-ANP32e and anti-H2A.Z, using the same chromatin, from a normal adult mouse heart, or that undergoing hypertrophic growth after transverse aortic constriction (TAC). The heatmaps of the sequencing tags aligned across the transcriptional start site (TSS), show that the two proteins co-localize at this position (Fig.

8a), while the graphs of the average peak values reveal subtle variations in the pattern of association during growth in the form of a forward movement of ANP32e, accompanied by an incremental increase in the 3′ *versus* 5′ H2A.Z peak encompassing the TSS (Fig. 8b). Furthermore, the 2D matrices of observed/expected distribution of H2A.Z and ANP32e at the TSS or in the gene body, show that the majority of both molecules co-localize at a frequency higher than expected by chance (red regions, Fig. 8c). This is further demonstrated by their binding patterns to individual genes, which also reveals that the levels of ANP32e at the TSS is differentially regulated after growth induction (Fig. 8d–g). Shown, are images of the distributions of the binding sites and densities of ANP32e and H2A.Z across H2A (Hist3h2a), Cdk7, and ribosomal S6 (Rps6) mouse housekeeping genes (ubiquitously expressed, essential genes). Pol II binding is included, to demarcate the TSS of genes and confirm active transcription. The images show that ANP32e is reduced at the TSS of H2A, as it is increases at that of Cdk7 (Fig. 8d–e, 8g). This could explain why, upon the knockdown of ANP32e during myocyte growth, H2A protein remained unchanged, while Cdk7 was reduced (Fig. 8c). Another pattern of change in ANP32e binding is observed at the TSS of ribosomal S6 protein, where there is a 5′ shift of its binding peak, to coincide with that of pol II and the +1 H2A.Z peaks (Fig. 8f). This would be consistent with the requirement of ANP32e for S6 transcription (Fig. 7b). On the other hand, the levels of H2A.Z remained relatively unchanged (Fig. 8g). The median and quartiles for the sequence Tags of pol II, H2A.Z, and ANP32e at the TSS (−1000 to + 1000) and gene bodies (+1000 to gene end) of the collective housekeeping (72.3%, with 0.75–1.3-fold change in pol II during growth, Fig. 8h), inducible (9.4%, with >1.3-fold increase in pol II during growth, Fig. 8i–j), tissue-specific (2.7%, Fig. 8k), and downregulated (15.5%, with <0.75-fold reduction in pol II during growth, Fig. 8l) genes, show that pol II, H2A.Z and ANP32e levels are highest at the housekeeping TSS, where pol II exhibits pause-release during growth (incremental reduction of pol II at the TSS with an equivalent increase in gene body), whereas, tissue-specific genes have the highest levels of pol II, H2A.Z, and Anp32e within their gene body, and the lowest at their TSS. In general, H2A.Z exhibits little changes during growth in any of the gene categories, while, Anp32e increases in a subset of inducible genes, decrease among other and on tissue-specific genes, but remains unchanged in downregulated genes, with no correlation to changes in pol II. These results demonstrate the co-localization of ANP32e and H2A.Z, for the most part, as particularly clear in their overlapping patterns of binding observed in the individual gene examples (Fig. 8d.–f., 8i–l.). Since chromatin-bound H2A.Z, for the most part, does not parallel changes in pol II binding, we predict the H2A.Z influences transcription through recruitment of Anp32e and plausibly other proteins that remain to be identified, while Anp32e influences proteins' activity/stability via inhibiting PP2A.

DISCUSSION

H2A.Z is known to positively regulate gene expression through destabilizing the +1 nucleosome and facilitating the progression of pol II across genes, a function that is largely consistent across various species. Additionally, it prevents DNA methylation across the gene bodies of inducible genes in *Arabidopsis,* thus, augmenting their responsiveness to stimuli. However, in spite of the emerging role of H2A.Z in disease development, including cancer

[36–38], HIV [39] and cardiac hypertrophy [22], we have limited knowledge regarding the mechanisms regulating its expression, under physiological or pathological conditions.

Posttranslational modifications are involved in modulating H2A.Z's function. This H2A variant is modified by acetylation at K4, K7, K11 [40], methylation at K4, K7 [41], and ubquitination at K120, K121, K125 in mammalian cells [42], and sumoylation at K126, K133 of Htz1 in yeast [43]. Whereas, acetylated H2A.Z is associated with euchromatin and actively transcribed genes [44], the ubiquitinated form is found at the transcriptionally silent heterochromatin [42]. On the other hand, sumoylation plays a role in double-stranded-breaks in yeast. However, in contrast to other histones (H2A, H2A.X, H3, H2B..etc), phosphorylation of H2A.Z has not been reported.

Others [16] and we show that ANP32e interacts with H2A.Z. Since ANP32e and other Anp32 family members are known to inhibit PP2A [32, 33, 45], it was pertinent to investigated whether H2A.Z is a target of phosphorylation. Our data show that H2A.Z is indeed phosphorylated and that this modification is dependent on ANP32e availability, which we also show is required for H2A.Z's stability. Since ANP32e interacts with the N-terminus of H2A.Z, we predicted that the site of phosphorylation is serine-9, the only putative phosphorylation site in the N-terminus. In support, mutations of this site resulted in an unstable protein that failed to localize to the nucleus, an effect similar to what we observe with knockdown of ANP32e. Ultimately, inhibition of PP2A in ANP32e depleted cells proved that the effects of ANP32e on H2A.Z's stability are mediated through inhibition of the phosphatase. Moreover, knockdown of MSK1, a nuclear kinase that has been shown to phosphorylate H3-S10 [35], mimicked the effects of ANP32e knockdown, suggesting that it maybe the kinase involved in phosphorylating H2A.Z.

In contrast to the stabilizing effect of ANP32e on H2A.Z that we demonstrate in this study, we have previously reported that the deacetylase, Sirt1, is involved in destabilizing H2A.Z and reducing its expression levels, which is dependent on both the N- and C-termini including lysine 15, 115, and 121 [22]. Thus, acetylation and phosphorylation are both required for stabilization of H2A.Z under different conditions that may involve nutrient availability, which regulates Sirt1 abundance, and growth factor stimulation, which regulates the phosphorylation status and activity of cellular proteins. Notably, neither ANP32e nor PP2A are restricted to the nucleus, but are equally or more abundantly present in the cytoplasm. As we show, knockdown of ANP32e almost completely inhibited FBS-induced phosphorylation of Erk1/2 and ribosomal S6 (Fig. 7). Therefore, it is plausible that their cytosolic functions may also indirectly impact nuclear H2A.Z stability and inclusion, and gene expression. This could also explain the differences in the functional effect of ANP32e knockdown on H2A.Z that we observed in cardiac myocytes vs. those observed by Obri et al [16] or Mao et al [17] in mouse embryonic fibroblasts (MEFs) and Hela cells, respectively. The difference being that the former are terminally differentiated primary cell types, while the latter are proliferating cell lines, with plausible differences in Anp32e distribution, H2A.Z:Anp32e stoichiometry, as well as, the presence of other unique interacting proteins and/or modifiers. The latter studies show that knockdown of ANP32e results in nucleosomal incorporation of H2A.Z at unique intergenic and enhancer sites [16], as well as, an increase H2A.z at the +1 nucleosome position, while the opposite is observed with its overexpression

[17], which suggests that ANP32e induces nucleosomal eviction of H2A.Z. In contrast, we show that knockdown of ANP32e in cardiac myocytes induces proteasomal degradation of H2A.Z, and reduces its nuclear content, while its overexpression had no apparent effect. Moreover, we find that the “new” H2A.Z-binding sites that are detected in ANP32e knockout MEFs (e.g. within the Ttc21a and Slc26a9 introns), are present in the normal heart genome, and are associated with endogenous ANP32e, or none in the case of Sox30 (Fig. 5S). This supports our conclusion that in the heart genome, the presence of Anp32e does not necessarily cause eviction of H2A.Z. One limitation of Obri et al’s study [16], is the lack of ChIP-Seq data for Anp32e that would allow us to contrast it with the appearance of the new H2A.Z binding sites. Although, one could argue that since our ChIP-Seq results are from whole organ chromatin, that the H2A.Z and ANP32e binding sites exist in different cell types, this would contradict the fact that ANP32e specifically binds H2A.Z. Another major difference between our study and that of Obri et al’s, is the interaction site of Anp32e. While, both studies show that the acidic C-terminal domain of Anp32e interacts with H2A.Z, we report the interaction to occur with the N-terminal tail of H2A.Z, as confirmed by the yeast-two-hybrid system, co-immunoprecipitation, and functional effects on recombinant fusion GFP proteins, and Obri et al report it to be with the αC-helix (a.a. 89–100), as confirmed by co-immunoprecipitation and x-ray crystallography. We have no good explanation for this discrepancy, except that maybe Anp32e can interact with both the N-terminal and αC-helix of H2A.Z, depending on the cell type and conditions. Moreover, x-ray crystallography may lack any necessary posttranslational modifications and/or other factors necessary for its interaction with the N-terminus.

As expected from the interaction of the two proteins, ChIP-Seq of chromatin from the heart tissue revealed the co-localization of H2A.Z and ANP32e across the genome, mainly at the TSSs of actively transcribed genes, but also in the gene bodies of a subset of inducible genes (Myc, Cyr61, Egr1..etc, Fig. 8i). Interestingly, ANP32e increased significantly at those sites after growth induction, while H2A.Z’s density, remaining relatively high, exhibited a minimal increase at peaks immediately downstream of the TSS (the +1 nucleosome position). One of the advantages of ChIP-Seq in whole organ, is capturing the binding of these factors in the native 3D environment, which can be substantially different from the dissociated monolayers of a homogenous cell type, especially as this is known to result in dedifferentiation of cardiac myocyte. On the other hand, this approach would represent the sum of changes in all constituent cell types. Notably, the heart is composed of ~40% cardiac myocytes by number, and >90% by volume. Thus, the product of expressed genes in the heart, including the ubiquitous, constitutive, housekeeping genes (72.3% of expressed genes in the heart), is expected to be proportional to the volume of constituent cells. Moreover, growth-inducible genes respond similarly in all the resident cell types (myocytes, endothelial, fibroblasts, and smooth muscle cells). Housekeeping gene in the heart, are regulated by a pause-release mechanism [29], may exhibit an a slight increase or decrease in ANP32e, but virtually no change in the relatively high levels of H2A.Z localized at the TSS. In contrast to housekeeping and inducible genes, most tissue-specific genes, which are constitutively expressed, have the highest levels of bound pol II, H2A.Z, and Anp32e within gene bodies, and the lowest levels at the TSS (Fig. 8k). Thus, what the data show, is that in any of the expressed genes, while H2A.Z exhibits none or minimal changes, changes in

Anp32e do not necessarily positively correlate with changes in pol II, which indicates that it that it may be exerting regulatory effects through, as of yet, unidentified factors, for example, such as those that regulate transcriptional elongation rates. It should also be noted, that we found that H2A.Z is also bound to ~14% of all genes that have no pol II (unexpressed), and this is associated with none to low levels ANP32e (Fig. 6S), suggesting that H2A.Z is also associated with restricted transcription, which is moderated by ANP32e, required for its stability, among other regulatory effects, not discounting its cytosolic effects on the phosphorylation of signaling proteins (Fig. 7).

In summary, 1) Anp32e knockdown induces downregulation of nuclear H2A.Z, this effect is rescued by epoxomicin, suggesting that it is a proteasomal-dependent degradation event. Since the rescued protein fails to localize to the nucleus, it suggests that Anp32e is also necessary for its nuclear inclusion, plausibly, through maintaining a post-translational modification. 2) The N-terminus of H2A.Z, is sufficient for conferring sensitivity to ANP32e, as knockdown of Anp32e significantly reduces recombinant zGFP in the cytosolic, as well as, the nuclear compartment. 3) Overexpression of PP2A, expressed mainly in the cytosol, with a minor component in the nucleus, induces gradation of endogenous nuclear H2A.Z and exogenously-delivered, as it coexists with PP2A in the cytosol and other cellular compartments. 4) Mutation of a unique Ser-9 in the N-terminus of H2A.Z, destabilizes the protein that can be rescued by epoxomicin, although it still fails to localize to the nucleus, while Anp32e knockdown inhibits H2A.Z phosphorylation. 5) Knockdown of Anp32e completely inhibits serum-stimulated phosphorylation of Erk and S6, supporting the fact that it is a PP2A inhibitor in the cytosol. 6) H2A.Z and Anp32e co-localize genome-wide on all expressed genes. However, with little changes in the abundance of H2A.Z during growth induction in the heart, changes in Anp32e are likely to exert its effect on transcriptional regulation through preventing H2A.Z dephosphorylation via PP2A, among other, as of yet, unidentified targets.

Acknowledgments

We thank Dr. Junichi Sadoshima, Chairman of the Department of Cell Biology and Molecular Medicine, Rutgers University, for his support.

FUNDING

The work was supported by National Institute of Health funding to the corresponding author, Maha Abdellatif (1R01HL119726), and Dr. Danish Sayed (1R01HL128799).

References

1. Allis CD, Richman R, Gorovsky MA, Ziegler YS, Touchstone B, Bradley WA, Cook RG. hv1 is an evolutionarily conserved H2A variant that is preferentially associated with active genes. J Biol Chem. 1986; 261:1941–1948. [PubMed: 3944120]
2. Meneghini MD, Wu M, Madhani HD. Conserved histone variant H2A.Z protects euchromatin from the ectopic spread of silent heterochromatin. Cell. 2003; 112:725–736. [PubMed: 12628191]
3. Li B, Pattenden SG, Lee D, Gutierrez J, Chen J, Seidel C, Gerton J, Workman JL. Preferential occupancy of histone variant H2AZ at inactive promoters influences local histone modifications and chromatin remodeling. Proc Natl Acad Sci U S A. 2005; 102:18385–18390. Epub 12005 Dec 18312. [PubMed: 16344463]

4. Zhang H, Roberts DN, Cairns BR. Genome-wide dynamics of Htz1, a histone H2A variant that poises repressed/basal promoters for activation through histone loss. Cell. 2005; 123:219–231. [PubMed: 16239141]
5. Raisner RM, Hartley PD, Meneghini MD, Bao MZ, Liu CL, Schreiber SL, Rando OJ, Madhani HD. Histone variant H2A.Z marks the 5′ ends of both active and inactive genes in euchromatin. Cell. 2005; 123:233–248. [PubMed: 16239142]
6. Krogan NJ, Keogh MC, Datta N, Sawa C, Ryan OW, Ding H, Haw RA, Pootoolal J, Tong A, Canadien V, Richards DP, Wu X, Emili A, Hughes TR, Buratowski S, Greenblatt JF. A Snf2 family ATPase complex required for recruitment of the histone H2A variant Htz1. Mol Cell. 2003; 12:1565–1576. [PubMed: 14690608]
7. Mizuguchi G, Shen X, Landry J, Wu WH, Sen S, Wu C. ATP-driven exchange of histone H2AZ variant catalyzed by SWR1 chromatin remodeling complex. Science. 2004; 303:343–348. Epub 2003 Nov 2026. [PubMed: 14645854]
8. Papamichos-Chronakis M, Watanabe S, Rando OJ, Peterson CL. Global regulation of H2A.Z localization by the INO80 chromatin-remodeling enzyme is essential for genome integrity. Cell. 2011; 144:200–213. doi:210.1016/j.cell.2010.1012.1021. [PubMed: 21241891]
9. Leach TJ, Mazzeo M, Chotkowski HL, Madigan JP, Wotring MG, Glaser RL. Histone H2A.Z is widely but nonrandomly distributed in chromosomes of Drosophila melanogaster. J Biol Chem. 2000; 275:23267–23272. [PubMed: 10801889]
10. Weber CM, Ramachandran S, Henikoff S. Nucleosomes are context-specific, H2A.Z-modulated barriers to RNA polymerase. Mol Cell. 2014; 53:819–830. doi:810.1016/j.molcel.2014.1002.1014. [PubMed: 24606920]
11. Fan JY, Rangasamy D, Luger K, Tremethick DJ. H2A.Z alters the nucleosome surface to promote HP1alpha-mediated chromatin fiber folding. Mol Cell. 2004; 16:655–661. [PubMed: 15546624]
12. Creyghton MP, Markoulaki S, Levine SS, Hanna J, Lodato MA, Sha K, Young RA, Jaenisch R, Boyer LA. H2AZ is enriched at polycomb complex target genes in ES cells and is necessary for lineage commitment. Cell. 2008; 135:649–661. doi:610.1016/j.cell.2008.1009.1056. Epub 2008 Nov 1016. [PubMed: 18992931]
13. Li Z, Gadue P, Chen K, Jiao Y, Tuteja G, Schug J, Li W, Kaestner KH. Foxa2 and H2A.Z mediate nucleosome depletion during embryonic stem cell differentiation. Cell. 2012; 151:1608–1616. doi: 1610.1016/j.cell.2012.1611.1018. [PubMed: 23260146]
14. Gevry N, Chan HM, Laflamme L, Livingston DM, Gaudreau L. p21 transcription is regulated by differential localization of histone H2A.Z. Genes Dev. 2007; 21:1869–1881. [PubMed: 17671089]
15. Wong MM, Cox LK, Chrivia JC. The chromatin remodeling protein, SRCAP, is critical for deposition of the histone variant H2A.Z at promoters. J Biol Chem. 2007; 282:26132–26139. Epub 22007 Jul 26138. [PubMed: 17617668]
16. Obri A, Ouararhni K, Papin C, Diebold ML, Padmanabhan K, Marek M, Stoll I, Roy L, Reilly PT, Mak TW, Dimitrov S, Romier C, Hamiche A. ANP32E is a histone chaperone that removes H2A.Z from chromatin. Nature. 2014; 505:648–653. doi:610.1038/nature12922. Epub 12014 Jan 12922. [PubMed: 24463511]
17. Mao Z, Pan L, Wang W, Sun J, Shan S, Dong Q, Liang X, Dai L, Ding X, Chen S, Zhang Z, Zhu B, Zhou Z. Anp32e, a higher eukaryotic histone chaperone directs preferential recognition for H2A.Z. Cell Res. 2014; 24:389–399. doi:310.1038/cr.2014.1030. Epub 2014 Mar 1011. [PubMed: 24613878]
18. Alatwi HE, Downs JA. Removal of H2A.Z by INO80 promotes homologous recombination. EMBO Rep. 2015; 16:986–994. doi:910.15252/embr.201540330. Epub 201542015 Jul 201540333. [PubMed: 26142279]
19. Sura W, Kabza M, Karlowski WM, Bieluszewski T, Kus-Slowinska M, Paweloszek L, Sadowski J, Ziolkowski PA. Dual Role of the Histone Variant H2A.Z in Transcriptional Regulation of Stress-Response Genes. Plant Cell. 2017; 29:791–807. doi:710.1105/tpc.1116.00573. Epub 02017 Mar 00573. [PubMed: 28258158]
20. Coleman-Derr D, Zilberman D. Deposition of histone variant H2A.Z within gene bodies regulates responsive genes. PLoS Genet. 2012; 8:e1002988. doi:1002910.1001371/journal.pgen.1002988. Epub 1002012 Oct 1002911. [PubMed: 23071449]

21. Zilberman D, Coleman-Derr D, Ballinger T, Henikoff S. Histone H2A.Z and DNA methylation are mutually antagonistic chromatin marks. Nature. 2008; 456:125–129. doi:110.1038/nature07324. Epub 02008 Sep 07324. [PubMed: 18815594]
22. Chen IY, Lypowy J, Pain J, Sayed D, Grinberg S, Alcendor RR, Sadoshima J, Abdellatif M. Histone H2A.z is essential for cardiac myocyte hypertrophy but opposed by silent information regulator 2alpha. J Biol Chem. 2006; 281:19369–19377. [PubMed: 16687393]
23. Sayed D, Yang Z, He M, Pfleger J, Abdellatif M. Acute Targeting of General Transcription Factor IIB Restricts Cardiac Hypertrophy via Selective Inhibition of Gene Transcription. Circ HF. 2015; 8:138–148.
24. Han M, Yang Z, Sayed D, He M, Gao S, Lin L, Yoon SH, Abdellatif M. GATA4 Expression is Primarily Regulated via a miR-26b-Dependent Posttranscriptional Mechanism During Cardiac Hypertrophy. Cardiovasc Res. 2012; 93:645–654. [PubMed: 22219180]
25. Sayed D, Hong C, Chen IY, Lypowy J, Abdellatif M. MicroRNAs play an essential role in the development of cardiac hypertrophy. Circ Res. 2007; 100:416–424. [PubMed: 17234972]
26. Lypowy J, Chen IY, Abdellatif M. An alliance between Ras GTPase-activating protein, filamin C, and Ras GTPase-activating protein SH3 domain-binding protein regulates myocyte growth. J Biol Chem. 2005; 280:25717–25728. [PubMed: 15886195]
27. Yue Y, Lypowy J, Hedhli N, Abdellatif M. Ras GTPase-activating protein binds to Akt and is required for its activation. J Biol Chem. 2004; 279:12883–12889. Epub 12004 Jan 12885. [PubMed: 14707121]
28. Rane S, He M, Sayed D, Vashistha H, Malhotra A, Sadoshima J, Vatner DE, Vatner SF, Abdellatif M. Downregulation of MiR-199a Derepresses Hypoxia-Inducible Factor-1{alpha} and Sirtuin 1 and Recapitulates Hypoxia Preconditioning in Cardiac Myocytes. Circ Res. 2009; 104:879–886. [PubMed: 19265035]
29. Sayed D, He M, Yang Z, Lin L, Abdellatif M. Transcriptional regulation patterns revealed by high resolution chromatin immunoprecipitation during cardiac hypertrophy. J Biol Chem. 2013; 288:2546–2558. doi:2510.1074/jbc.M2112.429449. Epub 422012 Dec 429410. [PubMed: 23229551]
30. Lerdrup M, Johansen JV, Agrawal-Singh S, Hansen K. An interactive environment for agile analysis and visualization of ChIP-sequencing data. Nat Struct Mol Biol. 2016; 23:349–357. doi: 310.1038/nsmb.3180. Epub 2016 Feb 1029. [PubMed: 26926434]
31. Nicol JW, Helt GA, Blanchard SG Jr, Raja A, Loraine AE. The Integrated Genome Browser: free software for distribution and exploration of genome-scale datasets. Bioinformatics. 2009; 25:2730–2731. [PubMed: 19654113]
32. Costanzo RV, Vila-Ortiz GJ, Perandones C, Carminatti H, Matilla A, Radrizzani M. Anp32e/Cpd1 regulates protein phosphatase 2A activity at synapses during synaptogenesis. Eur J Neurosci. 2006; 23:309–324. [PubMed: 16420440]
33. Santa-Coloma TA. Anp32e (Cpd1) and related protein phosphatase 2 inhibitors. Cerebellum. 2003; 2:310–320. [PubMed: 14964690]
34. Bialojan C, Takai A. Inhibitory effect of a marine-sponge toxin, okadaic acid, on protein phosphatases. Specificity and kinetics. Biochem J. 1988; 256:283–290. [PubMed: 2851982]
35. Thomson S, Clayton AL, Hazzalin CA, Rose S, Barratt MJ, Mahadevan LC. The nucleosomal response associated with immediate-early gene induction is mediated via alternative MAP kinase cascades: MSK1 as a potential histone H3/HMG-14 kinase. Embo J. 1999; 18:4779–4793. [PubMed: 10469656]
36. Baptista T, Graca I, Sousa EJ, Oliveira AI, Costa NR, Costa-Pinheiro P, Amado F, Henrique R, Jeronimo C. Regulation of histone H2A.Z expression is mediated by sirtuin 1 in prostate cancer. Oncotarget. 2013; 4:1673–1685. [PubMed: 24127549]
37. Kim K, Punj V, Choi J, Heo K, Kim JM, Laird PW, An W. Gene dysregulation by histone variant H2A.Z in bladder cancer. Epigenetics Chromatin. 2013; 6:34.doi: 10.1186/1756-8935-1186-1134 [PubMed: 24279307]
38. Svotelis A, Gevry N, Grondin G, Gaudreau L. H2A.Z overexpression promotes cellular proliferation of breast cancer cells. Cell Cycle. 2010; 9:364–370. Epub 2010 Jan 2028. [PubMed: 20023423]

39. Seu L, Mobley JA, Goepfert PA. CD4+ T cells from HIV-1 patients with impaired Th1 effector responses to Mycobacterium tuberculosis exhibit diminished histone and nucleoprotein signatures. Clin Immunol. 2017; 181:16–23. Epub 2017 May 1025. DOI: 10.1016/j.clim.2017.1005.1018 [PubMed: 28552470]
40. Boyne MT 2nd, Pesavento JJ, Mizzen CA, Kelleher NL. Precise characterization of human histones in the H2A gene family by top down mass spectrometry. J Proteome Res. 2006; 5:248–253. [PubMed: 16457589]
41. Binda O, Sevilla A, LeRoy G, Lemischka IR, Garcia BA, Richard S. SETD6 monomethylates H2AZ on lysine 7 and is required for the maintenance of embryonic stem cell self-renewal. Epigenetics. 2013; 8:177–183. doi:110.4161/epi.23416. Epub 22013 Jan 23416. [PubMed: 23324626]
42. Sarcinella E, Zuzarte PC, Lau PN, Draker R, Cheung P. Monoubiquitylation of H2A.Z distinguishes its association with euchromatin or facultative heterochromatin. Mol Cell Biol. 2007; 27:6457–6468. Epub 2007 Jul 6416. [PubMed: 17636032]
43. Kalocsay M, Hiller NJ, Jentsch S. Chromosome-wide Rad51 spreading and SUMO-H2A.Z-dependent chromosome fixation in response to a persistent DNA double-strand break. Mol Cell. 2009; 33:335–343. doi:310.1016/j.molcel.2009.1001.1016. [PubMed: 19217407]
44. Boskovic A, Bender A, Gall L, Ziegler-Birling C, Beaujean N, Torres-Padilla ME. Analysis of active chromatin modifications in early mammalian embryos reveals uncoupling of H2A.Z acetylation and H3K36 trimethylation from embryonic genome activation. Epigenetics. 2012; 7:747–757. doi:710.4161/epi.20584. Epub 22012 Jul 20581. [PubMed: 22647320]
45. Reilly PT, Yu Y, Hamiche A, Wang L. Cracking the ANP32 whips: important functions, unequal requirement, and hints at disease implications. Bioessays. 2014; 36:1062–1071. doi:1010.1002/bies.201400058. Epub 201402014 Aug 201400025. [PubMed: 25156960]

Highlights

- The N-terminus of H2A.Z interacts with the acidic domain of Anp32e in cardiac myocytes
- Anp32e reduces proteasomal degradation of H2A.Z though its N-terminus
- Anp32e prevents dephosphorylation of H2A.Z
- Anp32e inhibits PP2A-induced degradation of H2A.Z
- The binding sites of H2A.Z and Anp32e overlap in the heart's genome

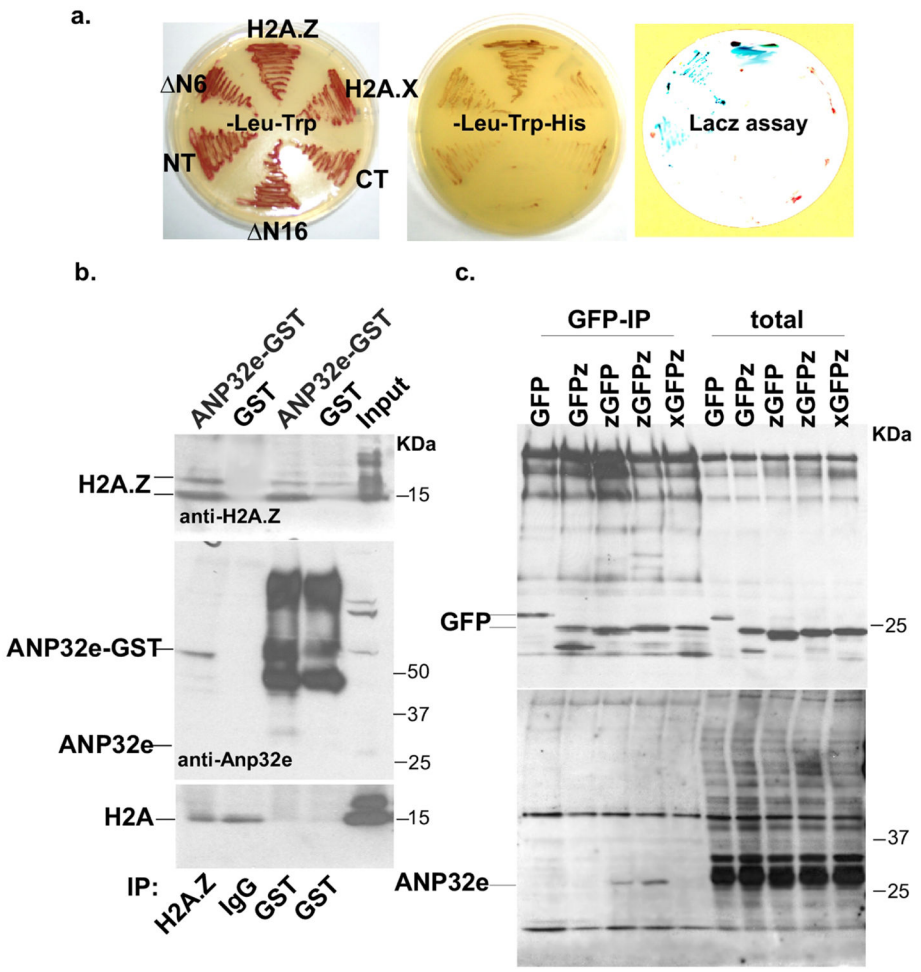

Figure 1. ANP32e interacts with H2A.Z

a. The bait plasmid vectors harboring fusion proteins of Gal4-DB with H2A.Z, H2A.X, the C-terminus of H2A.Z (CT), H2A.Z with a deletion of the N-terminal 16 aa (ΔN16), the N-terminal 16 aa (NT), or H2A.Z with a deletion of the N-terminal 6 aa (ΔN6), were transfected into the Y190 yeast strain along with the prey plasmid vector with the Gal4AD-ANP32e (nt 680–1070) fusion protein. The transfected yeast strain was streaked on medium deficient in leucine and tryptophan (-Leu-Trp), left plate, for selection of the cells that received both the bait and prey plasmids, or deficient in leucine, tryptophan, and histidine (-Leu-Trp-His), middle plate, for selection of cells that contain the bait and prey plasmids expressing fusion proteins that physically interact with one another. The colonies from the -Leu-Trp plate were also subjected to a filter-lift Lacz assay for confirming those interactions (right). b. Cardiac myocytes were transfected with plasmids harboring either GST or the GST-ANP32e fusing protein. After 24 h, cell lysates were subjected to immunoprecipitation with a rabbit polyclonal anti-GST, a mouse monoclonal anti-H2A.Z, or mouse IgG, as indicated. The immunoprecipitate was then analyzed by Western blotting using anti-H2A.Z, rabbit polyclonal anti-ANP32e, or anti-H2A, as indicated. The input is 1/20 the protein concentration that was used for immunoprecipitation. c. GFP fusion proteins with either the N-terminus domain of H2A.Z (zGFP), its C-terminal domain (GFPz), both domains

(zGFPz), or the N-terminal domain of H2A.X and the C-terminal domain of H2A.Z (xGFPz) were constructed and delivered to cardiac myocytes via adenoviral vectors. After 24 h, cell lysates were subjected to immunoprecipitation with anti-GFP and the immunoprecipitate analyzed by Western blotting using anti-GFP and anti-ANP32e, as indicated. In b. and c., the input is 1/20 the protein concentration used for immunoprecipitation (200 μg).

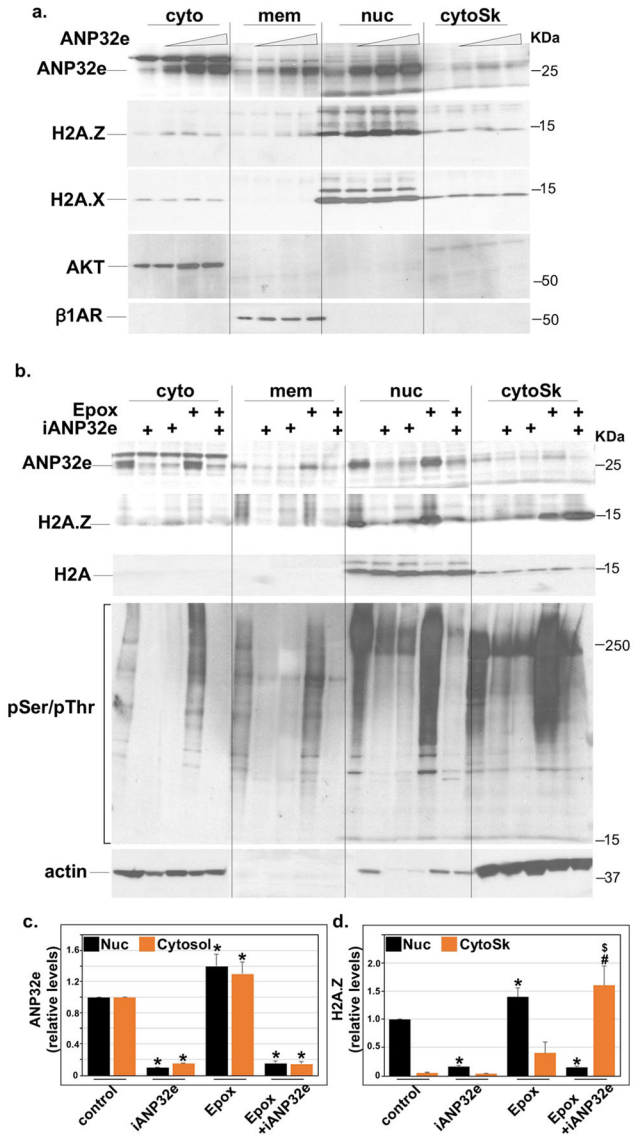

Figure 2. ANP32e is necessary for H2A.Z stabilization and nuclear localization

a. Increasing doses (moi 10, 20, 30) of ANP32e or Lacz (control) were delivered to cardiac myocytes via adenoviral vectors. After 24 h, the cells were lysed, fractionated into cytosol (cyto), membrane (mem), nuclear (nuc), and cytoskeletal (cytoSk) fractions, and analyzed by Western blotting using anti-ANP32e, -H2A.Z, -H2A.X, -AKT, and –β1AR, as indicated. b. Short-hairpin RNA targeting ANP32e (iANP32e, moi 10), or a control construct, was delivered to cardiac myocytes via adenoviral vectors, in the presence or absence of 0.1 μM epoxomicin (Epox). After 24 h, the cells were lysed, fractionated into cytosol, membrane, nuclear, and cytoskeletal fractions, and analyzed by Western blotting using anti-ANP32e, -H2A.Z, -H2A, -pSer/pThr, and –actin, as indicated. c. The ANP32e Western blot signals in the nuclear fraction in (b.), and d. H2A.Z signals in the nuclear (black bars) and cytoskeletal fractions (orange bars) in (b.), were quantitated, normalized to H2A or actin, respectively,

averaged, and plotted as relative levels (n=3). Error bars represent S.E.M., *$p<0.05$ v. nuclear control, # $p<0.05$ v. cytoSk control, $ $p<0.05$ v. Epox CytoSk.

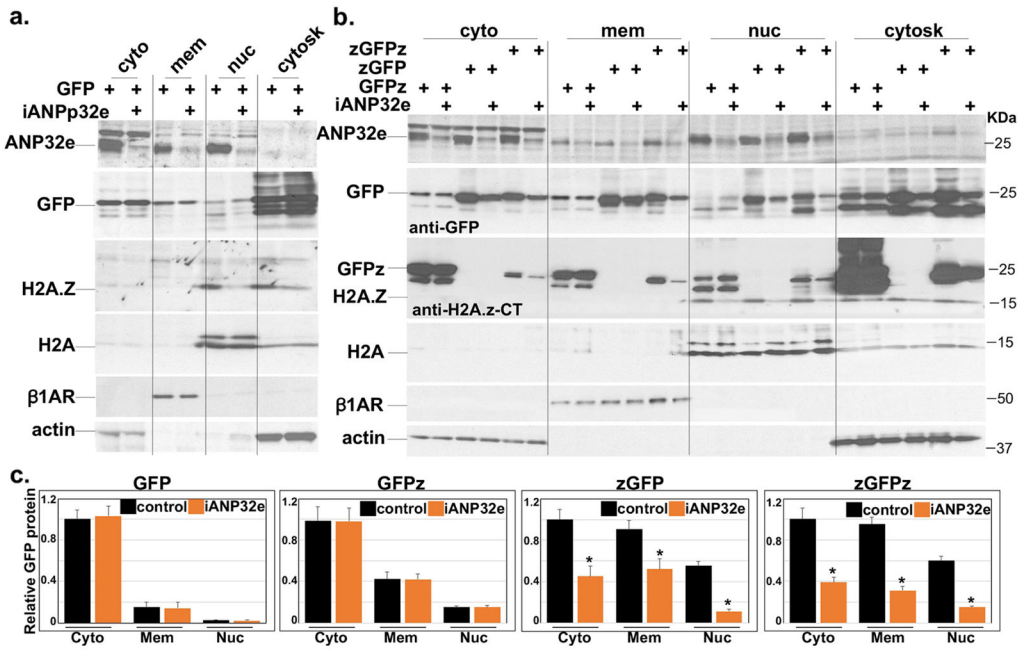

Figure 3. ANP32e-induced stabilization of H2A.Z is mediated through its N-terminal tail

a.–b. Short-hairpin RNA targeting ANP32e (iANP32e, where indicated by plus a + signs), or a control construct (unmarked lanes), was delivered to cardiac myocytes via an adenoviral vector. After 24 h, GFP or GFP fusion proteins with either the N-terminus domain of H2A.Z (zGFP), its C-terminal domain (GFPz), or both domains (zGFPz), were delivered to cardiac myocytes via adenoviral vectors, as indicated by plus a + signs. After 24 h, the cells were lysed, fractionated into cytosol (cyto), membrane (mem), nuclear (nuc), and cytoskeletal (cytoSk) fractions, and analyzed by Western blotting using anti-Anp32e, -GFP, -H2A.Z, -H2A, -beta1 adrenergic receptor (β1AR), and -actin, as indicated. c. Western blot signals for GFP, GFPz, zGFP, and zGFPz, in the absence (black bars) or presence (orange bars) of iANP32e, shown in a. and b., in the cytosol, membrane, and nuclear fractions, were quantitated, normalized to actin, β1AR, or H2A, respectively, averaged, and plotted as relative values (n=3), error bars represent S.E.M, *p<0.01 v. control.

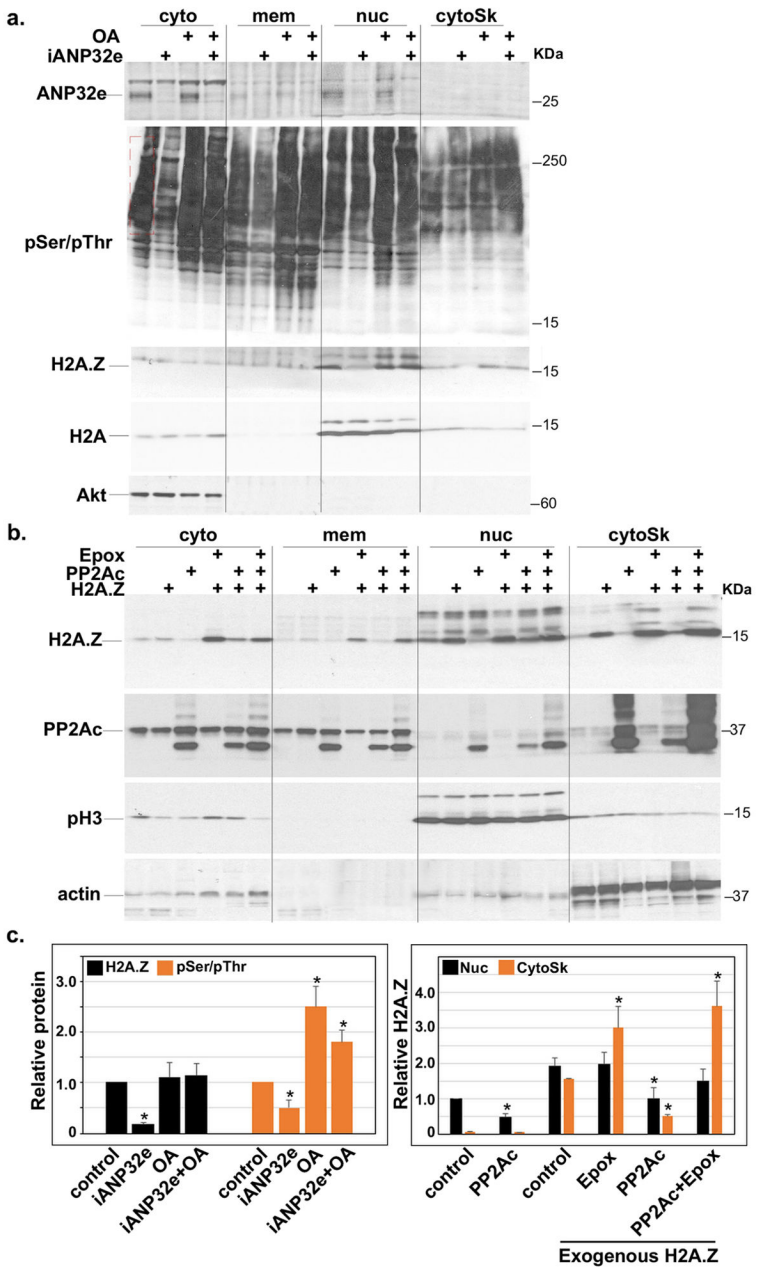

Figure 4. PP2A mediates the effects of ANP32e

a. Short-hairpin RNA targeting ANP32e (iANP32e, moi 10), or a control construct, was delivered to cardiac myocytes via adenoviral vectors, in the presence or absence of 10 nM okadiac acid (OA). After 24 h, the cells were lysed, fractionated into cytosol, membrane, nuclear, and cytoskeletal fractions, and analyzed by Western blotting using anti-ANP32e, -pSer/pThr, -H2A.Z, -H2A, and -AKT, as indicated. **b.** PP2A, with or without H2A.Z, or a control construct, were delivered to cardiac myocytes via adenoviral vectors (moi 10), in the presence or absence of 0.1 μM epoxomicin (Epox). After 24 h, the cells were lysed, fractionated into cytosol (cyto), membrane (mem), nuclear (nuc), and cytoskeletal (cytoSk) fractions, and analyzed by Western blotting using anti-H2A.Z, -PP2A, -pH3, and -actin, as

indicated. **c.** Left graph, the H2A.Z and pSer/pThr signals in the nuclear fractions of the images in (a.) were quantitated, normalized to H2A, and graphed as relative values (n=3). **c.** Right graph, the H2A.Z signal in the nuclear and cytoskeletal fraction of the images in (b.) were quantitated, normalized to pH3 or actin, respectively, and graphed as relative values (n=3). Error bars represent S.E.M., *p<0.05 v. control.

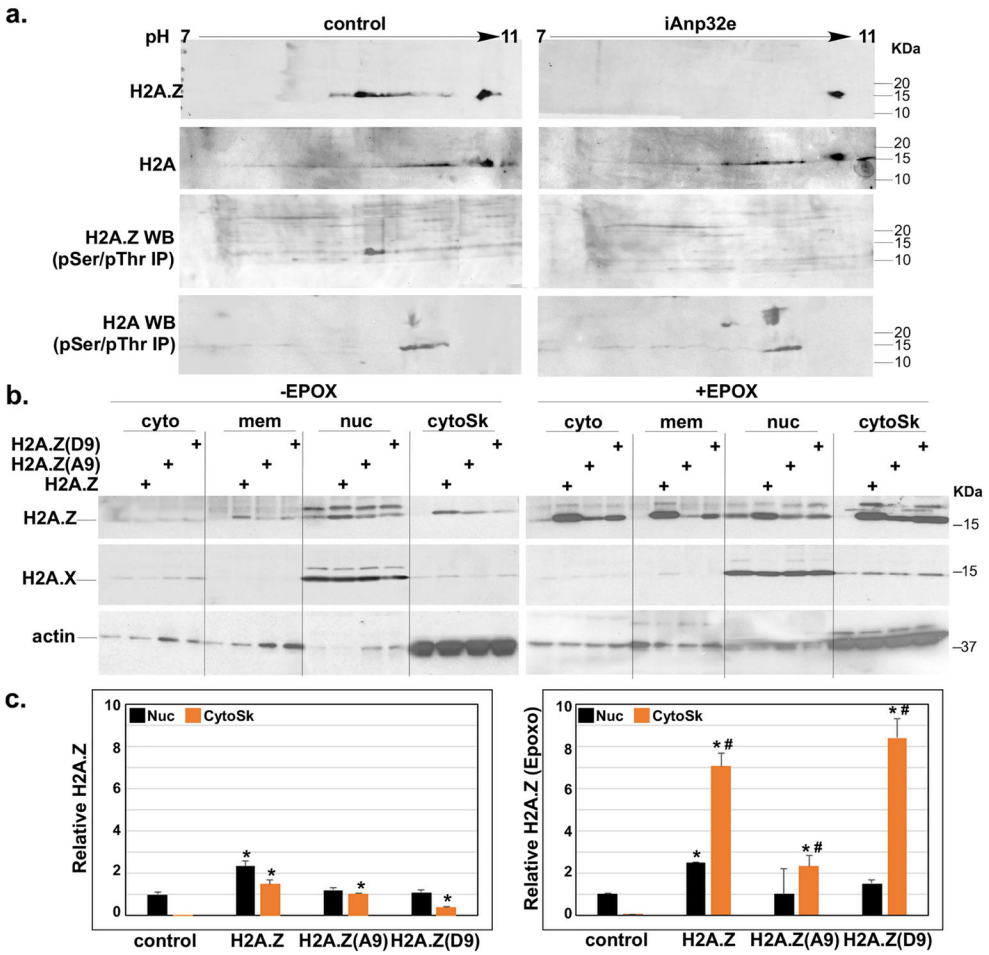

Figure 5. Knockdown of ANP32e destabilized H2A.Z and inhibits its phosphorylation

a. Short-hairpin RNA targeting ANP32e (iANP32e, moi 10), or a control construct, was delivered to cardiac myocytes via adenoviral vectors. After 24 h, histones were acid extracted. Total histones (top 2 panels), or those immunoprecipitated with a pSer/pThr antibody (lower 2 panels), were separated by 2D gel electrophoresis followed by blotting with anti-H2A.Z or anti-H2A (n=2). **b.** Wild type H2A.Z, or Ser9 mutants, H2A.Z (A9 or D9, moi 10), in the presence or absence of 0.1 μM epoxomicin (EPOX). After 24 h, the cells were lysed, fractionated into cytosol (cyto), membrane (mem), nuclear (nuc), and cytoskeletal (cytoSk) fractions, and analyzed by Western blotting using anti-H2A.Z, -H2A.X, and -actin, as indicated. **c.** The H2A.Z signal in the nuclear and cytoskeletal fraction of the images in (b.) were quantitated, normalized to H2A.X or actin, respectively, and graphed as relative values (n=3). Error bars represent S.E.M., *p<0.05 v. control of equivalent fraction, #p<0.05 v. nuclear control.

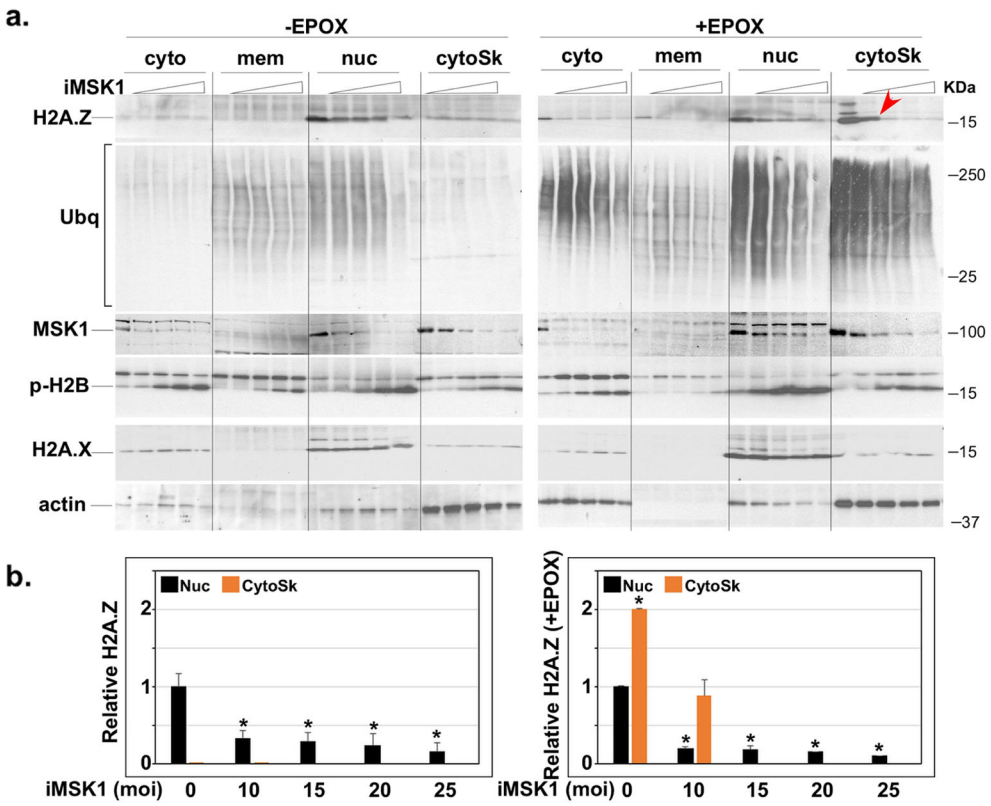

Figure 6. Knockdown of MSK1 induces degradation of H2A.Z

a. Short-hairpin targeting MSK1 (iMSK1), or a control construct, was delivered to cardiac myocytes (moi 10, 15, 20, 30), in the presence or absence of 0.1 μM epoxomicin (EPOX). After 24 h, the cells were lysed, fractionated into cytosol (cyto), membrane (mem), nuclear (nuc), and cytoskeletal (cytoSk) fractions, and analyzed by Western blotting using anti-H2A.Z, -ubiquitin, -MSK1, -pH2B, -H2A.X, and actin, as indicated. **b.** The H2A.Z signal in the nuclear and cytoskeletal fraction of the images in (a.) were quantitated, normalized to H2A.X or actin, respectively, and graphed as relative values (n=3). Error bars represent S.E.M., *p<0.05 v. nuclear control.

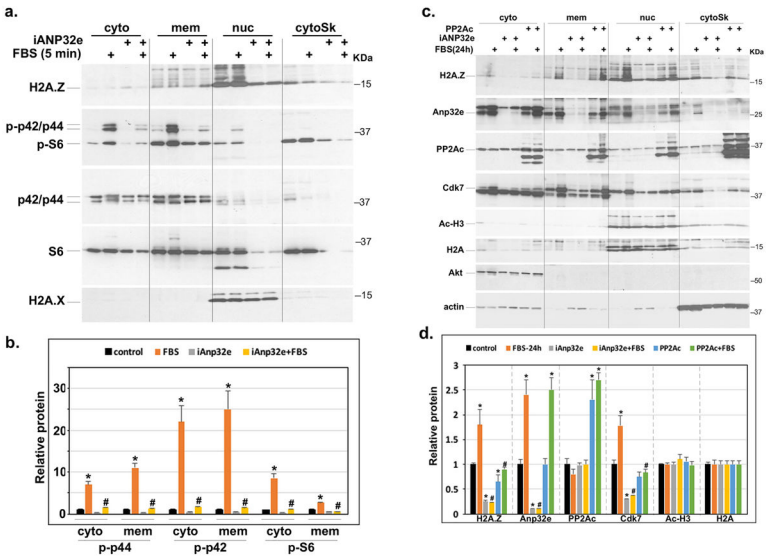

Figure 7. ANP32e is required for FBS-induced phosphorylation of Erk1/2 and S6, and selective gene expression

a. Short-hairpin RNA targeting ANP32e (iANP32e, moi 10), or a control construct, was delivered to cardiac myocytes via adenoviral vectors. After 24 h, the cells were either stimulated or not with 10%FBS for 5 minutes, before they were lysed, and fractionated into cytosol (cyto), membrane (mem), nuclear (nuc), and cytoskeletal (cytoSk) fractions, and analyzed by Western blotting using anti-H2A.Z, -phospho-p42/p44 (p-p42/p44), -phospho-S6 (p-S6), and -H2A.X, as indicated. **b.** The p-p42/p44 and pS6 signals in the cytosolic fraction were quantitated, normalized to total p42/p44 and S6, respectively, and graphed as relative values (n=3). Error bars represent S.E.M., *p<0.05 v. control, #p<0.05 *v.* FBS-stimulated. **c.** Short-hairpin RNA targeting ANP32e (iANP32e, moi 10), PP2A catalytic subunit (PP2Ac), or a control construct, were delivered to cardiac myocytes via adenoviral vectors. After 24 h, the cells were either stimulated, or not, with 10%FBS for 24 h, before they were lysed, and fractionated into cytosol (cyto), membrane (mem), nuclear (nuc), and cytoskeletal (cytoSk) fractions, and analyzed by Western blotting using anti-H2A.Z, -ANP32e, -PP2Ac, -Cdk7, -Ac-H3, -H2A, -Akt, and -actin, as indicated. **d**. The H2A.Z, ANP32e, PP2Ac, Cdk7, and Ac-H3 in the nuclear fraction were quantitated, normalized to H2A, and graphed as relative values (n=3). Error bars represent S.E.M., *p<0.05 v. control, #p<0.05 *v.* FBS-stimulated.

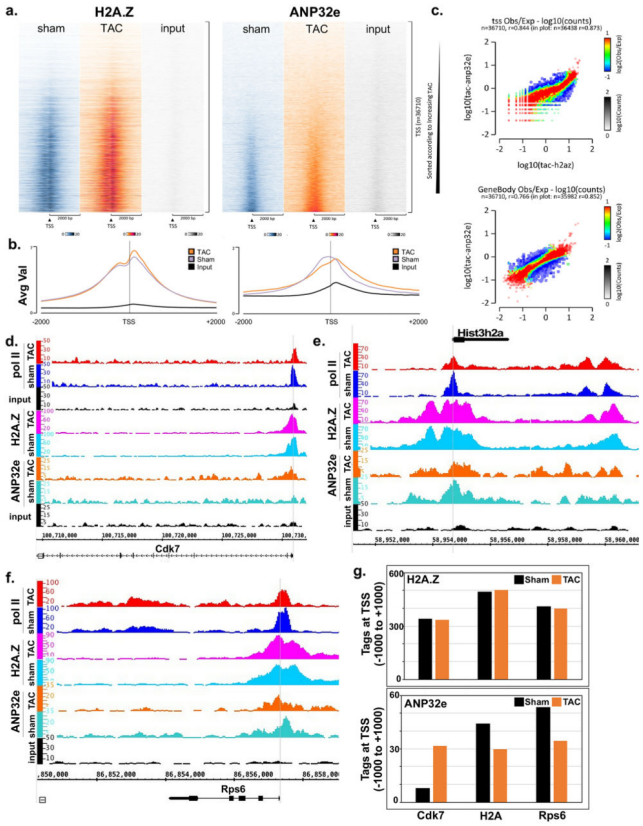

Figure 8ag

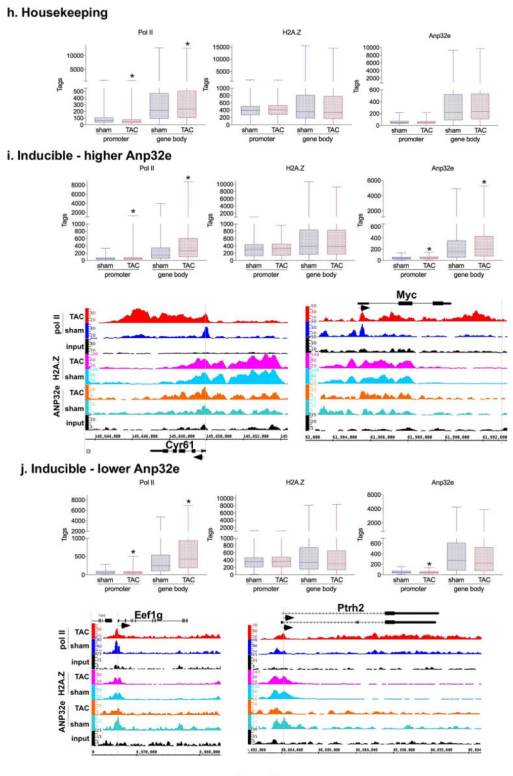

Figure 8hj

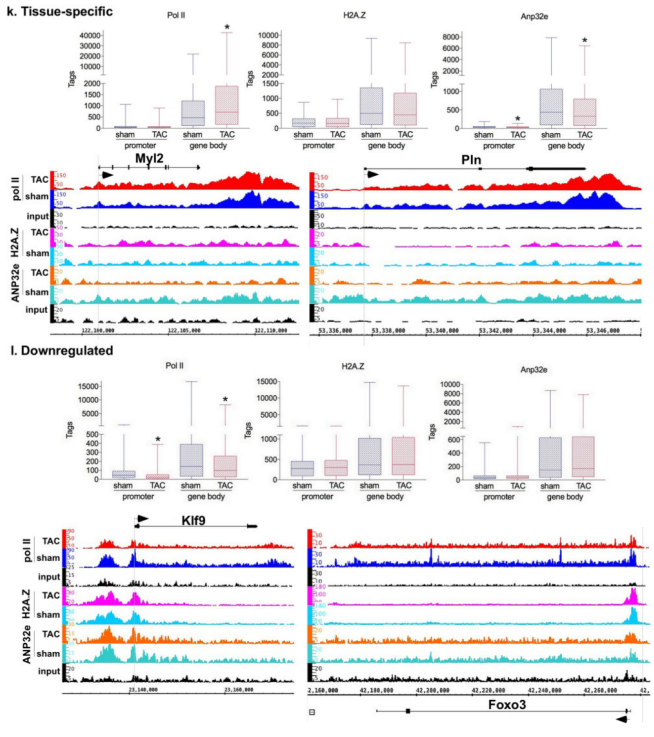

Figure 8kl

Figure 8. Co-localization of H2A.Z and ANP32e at the TSS of transcriptional active and inactive genes

Mice were subjected to a sham or transverse aortic constriction surgical (TAC) operation. One week post-TAC, the hearts were isolated and subjected to pol II, H2A.Z, and ANP32e ChIP-Seq. **a.** Heat maps of the H2A.Z and ANP32e ChIP-Seq sequence fragments from sham, TAC, and input at the TSS. The Y-axis represents individual positions of bins, and the X-axis represents a region from −2000 to +2000 bp relative to the TSS. **b.** Graphs representing average peak values of H2A.Z and ANP32e ChIP-Seq fragments from sham, TAC, and input from −2000 to +2000 bp relative to the TSS. **c.** Histograms showing the distribution of fragments calculated from their overall frequencies in the 'tac-h2az' (on X-axis) v. 'tac-ANP32e' (on Y-axis) within the TSS (upper) and gene body (lower) regions. The X and Y-axes were segmented into 75 bins, and the number of fragments within each bin was counted, color coded, and plotted. The bar to the right of the plot illustrates the relationship between count and coloring. The plots represent pseudo-colored 2D matrices showing observed/expected distribution calculated from the overall frequencies of fragments on each of the axes. This plot shows the relation between H2A.Z and ANP32e levels relative to what is expected if they occurred by chance. The pseudo-color corresponds to the Obs/Exp ratio, and the color intensity is proportional to the log2 of the number of observed fragments within each bin. These plots suggest that there is a positive correlation between the levels of H2A.Z and ANP32e, where the red indicates that this occurs more frequently than expected by chance. This plot also shows that regions that have the lowest levels of ANP32e and highest levels of H2A.Z, or conversely, those with the lowest levels of H2A.Z and highest ANP32e, occur less frequently than expected by chance (blue). **d.–f.** The plots represent ChIP-Seq results for Cdk7, Hist3h2a, and Rps6, for which the sequence fragments of pol II, H2A.Z, and ANP32e are aligned across the gene coordinates in Integrated Gene Browser (IGB). **g**. A graph representing total H2A.Z and ANP32e sequence tags at the TSS of Cdk7, Hist3h2a, and Rps6. Genes were sorted in **h.** housekeeping, **i.** inducible-higher Anp32e, **j.** inducible-lower Anp32e, **k.** tissue-specific, and **l.** downregulated gene groups, sorted according to the changes in pol II densities during TAC vs. sham, both at the TSS and gene bodies. Sequence Tags are represented as box plots for the median, quartiles, minimum, and maximum number of Tags. The images represent the densities of pol II, H2A.Z, and ANP32e sequence tags for Cyr61, Myc, Eef1g, Ptrh2, Myl2, and Pln, Klf9, Foxo3, aligned across the gene coordinates, using integrated genome browser (IGB).